DESIGN AND INSERTION PERFORMANCE OPTIMISATION OF A COMPOSITE INSERTION PIN FOR A CORN STALK SAND BARRIER LAYING DEVICE

/

玉米秸秆沙障铺设装置复合插针设计及插入性能优化

Qidong SUN, Weiqiang ZHENG*), Liping ZHANG, Bolin LI, Zhiqiang FENG, Senyu NIU, Chengqian XIE
College of Mechanical Engineering, Xinjiang University, Urumqi 830046 / China
Tel: +86-17733853240; E-mail: xjzwq@xju.edu.cn
DOI: https://doi.org/10.35633/inmateh-79-60

Keywords: *Axial insertion, composite insertion pin, corn stalk, discrete element method, insertion force stiffness, response surface methodology*

ABSTRACT

To address the problems of unstable posture, end crushing, and poor release during conventional press-in sand barrier laying caused by the large diameter, rigid internodes, pronounced nodes, and heterogeneous structure of corn stalks, a smooth composite insertion pin consisting of a front steel pin and a rear sleeve was designed. Based on the structural characteristics of the corn stalk rind, pith, and nodes, a layered discrete element model was established to analyze pith compression, sidewall friction, and local failure during axial insertion. The sleeve contact-segment diameter, steel pin diameter, and sleeve front transition angle were selected as experimental factors, and insertion force stiffness was adopted as the evaluation index. A Box-Behnken response surface design was employed for parameter optimization, followed by internodal validation, finite element analysis, nodal insertion tests, and release tests. The results showed that the sleeve contact-segment diameter had the greatest influence on insertion force stiffness, while the steel pin diameter and transition angle also had significant effects. The regression model exhibited a good fit, and the lack-of-fit was not significant. Considering machining feasibility and structural stability, the optimal structural parameters were a sleeve contact-segment diameter of 5.5 mm, a steel pin diameter of 2.0 mm, and a sleeve front transition angle of 160°, corresponding to a predicted insertion force stiffness of 1.15 N/mm. The validation results agreed well with the model predictions. Although the insertion force increased substantially in the nodal region, the optimized composite insertion pin successfully achieved axial insertion through the nodes and enabled smooth release in both the internodal and nodal regions.

摘要

针对玉米秸秆直径大、节间硬、结节明显及组织非均质导致传统压入式沙障铺设中姿态不稳、端部压溃和脱落不畅等问题，设计了由前端钢针和后部套筒组成的光滑复合插针。基于玉米秸秆表皮、内瓤和结节的结构特征，建立分层复合离散元模型，分析轴向插入过程中的内瓤压缩、侧壁摩擦和局部破坏行为。以套筒接触段直径、钢针直径和套筒前端变径角为试验因素，以插入力刚度为评价指标，开展 Box–Behnken 响应面优化，并通过普通节间验证、有限元分析、结节插入试验和脱落试验进行验证。结果表明，套筒接触段直径影响最显著，钢针直径和变径角也具有显著影响；模型拟合良好，失拟项不显著。综合考虑加工可行性和结构稳定性，推荐参数分别为 5.5 mm、2.0 mm 和 160°，预测插入力刚度约为 1.15 N/mm。普通节间验证结果表明，实测值与预测值吻合良好；虽然结节处插入力明显增大，但优化后的复合插针仍可完成结节处轴向插入，并能在普通节间和结节位置顺利脱落。

INTRODUCTION

Sand barrier laying is an important engineering measure for desertification control, wind-sand protection and ecological restoration in sandy areas (*Chen et al., 2024*). Its laying quality directly affects near-surface wind-speed reduction, sand-transport flux, surface stability and vegetation recovery. Among different sand-control measures, straw checkerboard sand barriers have been widely used in mobile sandy land, railway and highway protection, and ecological restoration projects because of their accessible materials, simple structure and stable sand-fixing effect. Previous studies have shown that sand barriers improve windbreak and sand-fixation performance by increasing surface roughness, modifying the near-surface airflow structure and weakening aeolian sand transport capacity (*Zhao et al., 2016; Wang et al., 2018; Zhang et al., 2018; Fang et al., 2023; Sun et al., 2024*). Semi-buried sand barriers, plate-type barriers, mesh barriers and porous sand-fixing components have also been developed to improve protective performance.

Their structural size, porosity, arrangement pattern and spacing can significantly affect wind-speed distribution, sediment deposition and sand-blocking efficiency (*Zhao et al., 2016; Wang et al., 2018; Fang et al., 2023; Sun et al., 2024; Xu et al., 2021; Zhang et al., 2021; Wang et al., 2024; Liu et al., 2025*).

With the development of wind-sand control engineering from manual construction towards mechanized, equipment-based and efficient operation, improving the laying quality and working efficiency of sand barriers has become an important research direction in desertification-control equipment (*Qu et al., 2019; Xu et al., 2020; Zhang et al., 2022*).

At present, most sand barrier laying machines have been developed for slender and flexible straw materials, such as wheat straw and reed straw. Conventional laying devices usually use inserting blades, pressing wheels, pressing discs or feeding–guiding mechanisms to press straw into sandy soil, forming sand barrier structures with a certain buried depth and exposed height. Related studies have shown that the mechanism type, feeding mode, pressing depth, working speed and straw feeding uniformity affect the forming quality of sand barriers and the straw mass per unit length (*An et al., 2025; Qi et al., 2025*). However, most existing machines are designed for flexible straw, and their working principle mainly depends on straw bending and overall pressing. For corn stalks with larger diameters, more rigid internodes and pronounced nodes, direct use of the conventional press-in method may easily cause unstable bending, poor posture control, end crushing, local splitting and poor release. Therefore, designing a key end-effector suitable for axial insertion and directional conveying according to the structural characteristics of corn stalks is fundamental for realizing mechanized laying of corn stalk sand barriers.

Corn stalk is a typical heterogeneous biological material consisting of nodes and internodes. Its cross-section includes a dense outer rind, vascular bundles and loose inner pith. Its mechanical properties are strongly affected by loading direction, moisture content, sampling position and stalk posture. Previous studies have shown that the corn stalk rind has relatively high tensile strength and stiffness, whereas the pith is loose and prone to compression, shearing and local failure (*Zhang et al., 2016; Chen and Qu, 2017; Zhang et al., 2020*). In addition, probe geometry, cross-sectional geometry and flexural stiffness affect puncture resistance, failure location and load-bearing capacity of corn stalks (*Robertson et al., 2016; Cook et al., 2020; Stubbs et al., 2022*). These studies provide a basis for understanding the mechanical behavior of corn stalks. Nevertheless, most of them focus on tension, bending, puncture, shearing or lodging, while limited attention has been paid to axial insertion, compression, friction and release of corn stalks during sand barrier laying.

During axial insertion of corn stalks, complex contact interactions occur between the insertion pin and the stalk pith. The front end of the pin first penetrates and compresses the loose pith. Subsequently, the pith is continuously squeezed and sheared. As the insertion depth increases, the contact length between the sidewall of the insertion pin and the pith increases, resulting in increased frictional resistance. When the insertion pin approaches a node, the dense tissue and transverse diaphragm increase local puncture, compression and shear resistance, causing obvious fluctuations or peaks in the insertion force curve. If the insertion pin diameter is too large, pith compression and sidewall friction increase significantly. If the diameter is too small, the supporting and guiding effects of the insertion pin are insufficient, leading to unstable stalk posture. Therefore, the structural parameters of the insertion pin should be optimized by comprehensively considering low-resistance insertion, stable holding and smooth release.

The discrete element method (DEM) can describe the contact, bonding, failure and motion processes of particulate materials, and has been increasingly applied to plant-material modelling, straw crushing, conveying and contact behavior analysis in recent years (*Coetzee, 2017; Zhang et al., 2020*). Meanwhile, response surface methodology is suitable for analyzing coupled effects among multiple factors and establishing regression relationships between structural parameters and performance indicators, and has been applied in the structural parameter optimization of agricultural equipment (*Myers et al., 2016; Montgomery, 2017; An et al., 2025; Qi et al., 2025*).

Based on this, a smooth composite insertion pin consisting of a front steel pin and a rear sleeve was designed for a corn stalk sand barrier laying device. The structural characteristics of corn stalks and the failure mechanism during axial insertion were analyzed, and a layered composite DEM model and an axial force model of the composite insertion pin were established. Then, the sleeve contact-segment diameter, steel pin diameter and sleeve front transition angle were selected as the main factors, and insertion force stiffness was used as the response value for Box-Behnken response surface optimization. Finally, direct internodal insertion validation, finite element analysis, nodal insertion tests and release verification tests were conducted to evaluate the prediction accuracy, structural stability and functional adaptability of the optimized structure.

MATERIALS AND METHODS

STRUCTURAL CHARACTERISTICS OF CORN STALK AND FAILURE MECHANISM DURING AXIAL INSERTION

Structural characteristics of corn stalk

Corn stalks are composed of nodes and internodes. The node is characterized by annular protrusions and contains a transverse diaphragm, with relatively dense tissue, whereas the internode is approximately cylindrical. In the cross-section, the stalk consists of a dense outer rind, vascular bundles and loose pith from the outside to the inside. The vascular bundles gradually become sparser from the outer region toward the center, forming a heterogeneous structure with a dense outer layer and a loose inner core, as shown in Figure 1.

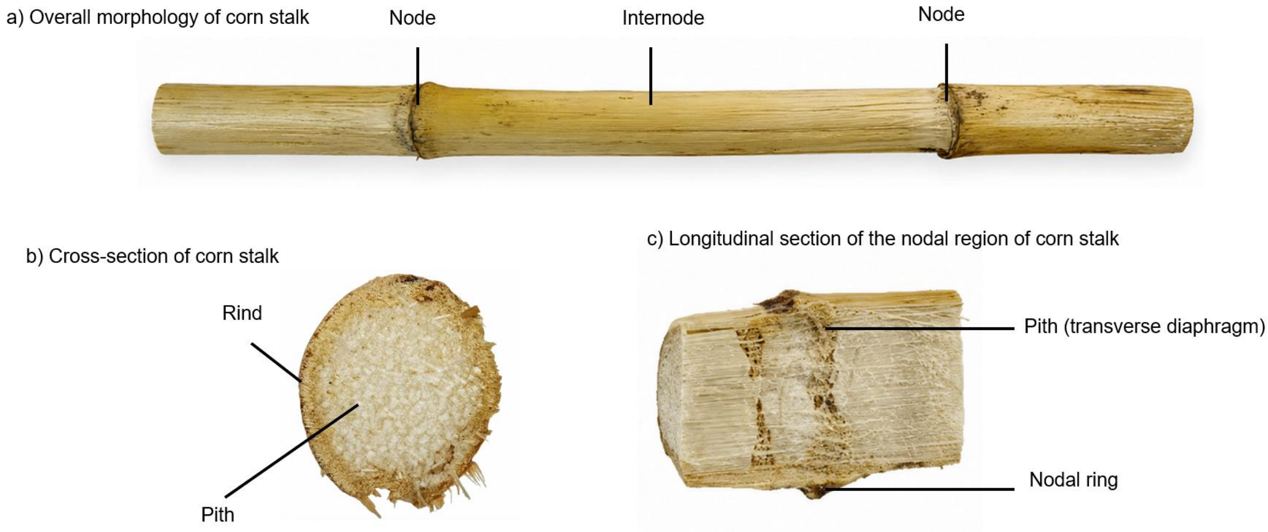

Fig. 1 - Morphological structure and nodal tissue characteristics of corn stalk

Discrete element representation of the layered structure of corn stalk

According to the structural differences among the rind, pith and nodal tissues, corresponding particle units were constructed and assigned material parameters and inter-particle bonding parameters for different regions, thereby forming a layered composite corn stalk model. The discrete element method (DEM) can describe inter-particle contact force transmission and local failure processes, and has been widely used to simulate the mechanical behavior of agricultural materials (Cundall and Strack, 1979; Tsuji et al., 1992). In recent years, many studies have optimized DEM parameter calibration and particle contact models, improving the simulation accuracy of plant materials (*Zhu et al., 2007*). In addition, DEM parameter calibration methods and model reliability evaluation have been systematically investigated (*Coetzee, 2017*). The model established in this study was used to characterize the structural differences between internodes and nodes, as well as local compression and failure behavior during insertion. The modelling process is shown in Figure 2.

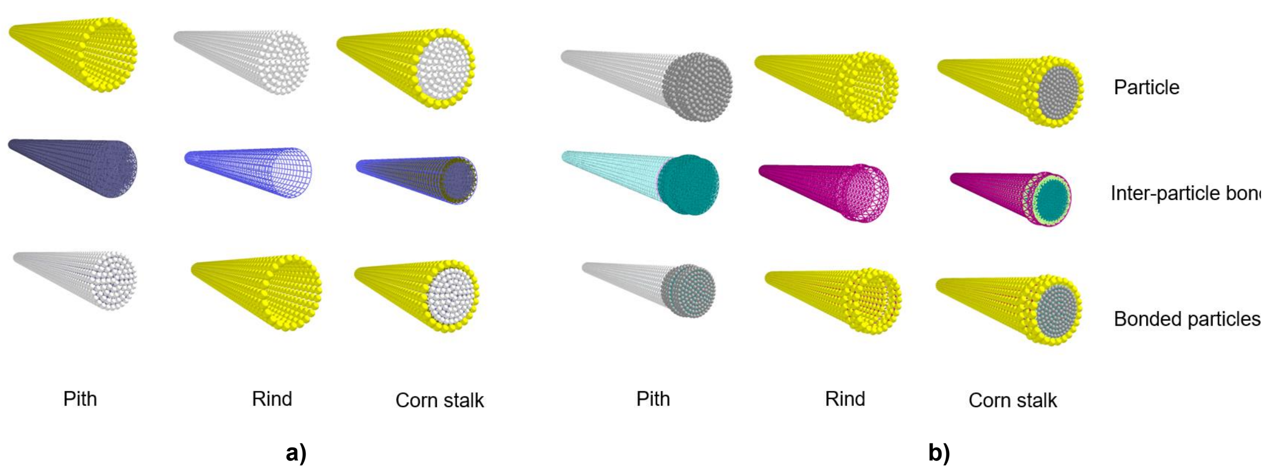

Fig. 2 - Construction process of the corn stalk discrete element model
a) internode model; b) nodal model

Analysis of insertion-induced failure modes

During axial insertion of corn stalks, the main failure modes include end crushing, pith compression, fiber shearing and nodal obstruction. The insertion pin first compresses the loose pith. Subsequently, the pith is continuously squeezed and sheared, while the sidewall friction increases with the contact length. When the pin approaches a node, the dense tissue and transverse diaphragm increase the local puncture and shear resistance, causing fluctuations or peaks in the insertion force curve. A typical process is shown in Figure 3. Therefore, the composite insertion pin should be designed to reduce the front penetration resistance and sleeve frictional resistance, while ensuring bending stability under lateral eccentric loading.

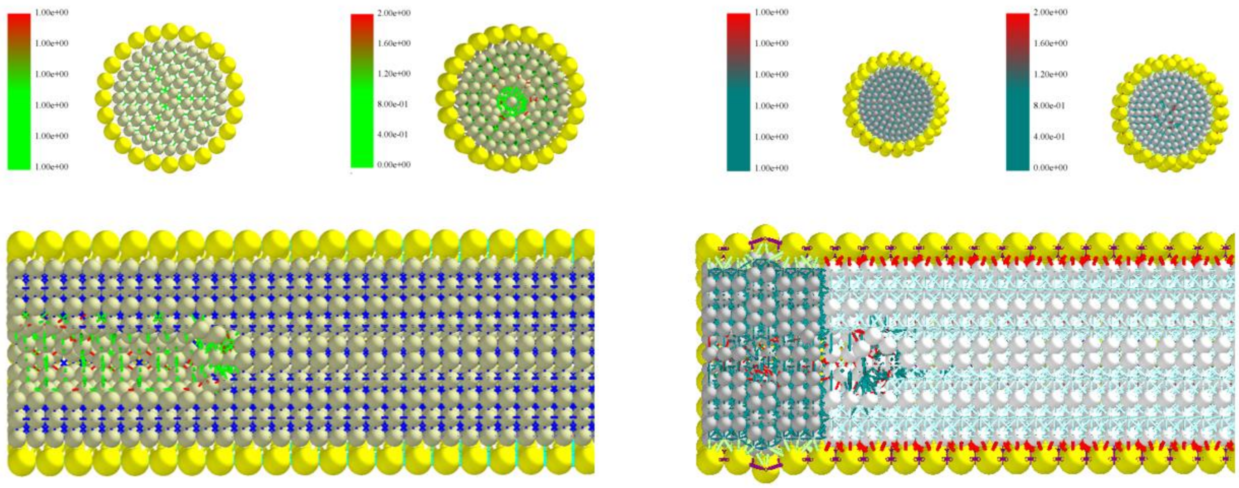

a) b)

Fig. 3 - Compression and failure characteristics of corn stalk pith during axial insertion
a) failure characteristics of internode; b) failure characteristics of nodal region

STRUCTURAL DESIGN OF THE INSERTION PIN

Design of the smooth composite insertion pin

The composite insertion pin was designed to realize axial insertion and directional conveying of corn stalks. Its design should ensure low-resistance penetration, stable holding and smooth release. In this study, a structure consisting of a front steel pin and a rear sleeve was adopted. The steel pin was used to penetrate and compress the pith and provide axial support, while the sleeve was used to fix the steel pin and connect it to the conveying mechanism. A gradual diameter transition was arranged between the two parts to reduce abrupt changes in contact resistance and improve the smoothness of load transmission. As shown in Figure 4, the corn stalk was sleeved along the axial direction of the insertion pin under the action of the push block. The thrust of the push block mainly overcame pith compression, local shearing and sidewall friction resistance. In addition, uneven stalk ends and non-uniform internal tissues may cause lateral eccentric loading.

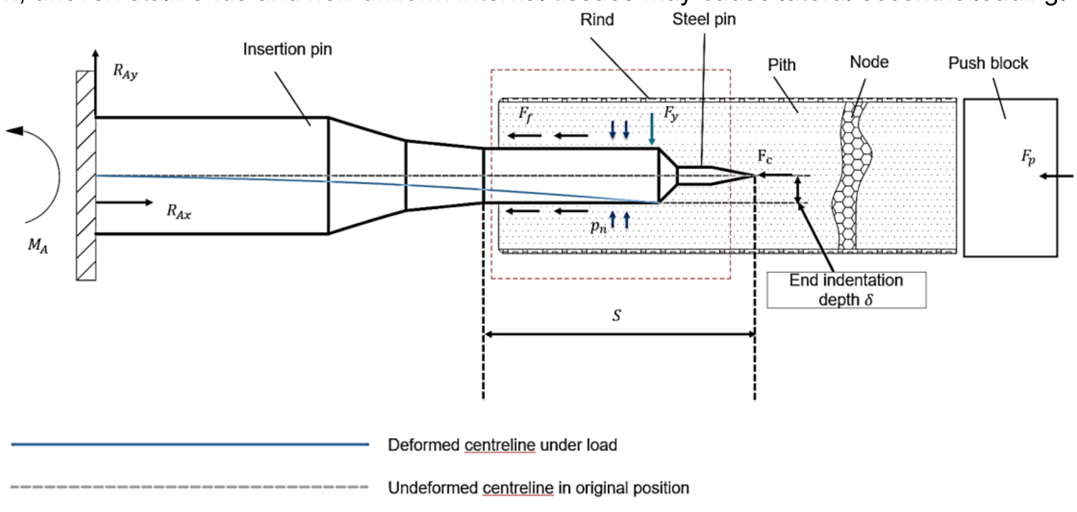

Fig. 4 - Force analysis of the composite insertion pin

In Figure 4, F_p represents the thrust of the push block; F_c represents the resistance caused by compression, squeezing and local shearing of the corn stalk pith; F_f represents the frictional resistance between the sidewall of the insertion pin and the stalk pith; P_n represents the radial normal pressure; and S represents the insertion depth of the stalk. R_{Ay}, R_{Ax}, M_A and F_y denote the vertical reaction force, axial reaction force, bending moment at the fixed end, and lateral force caused by eccentric loading, respectively, which are used to describe the possible non-axial loads during insertion.

Determination of key structural parameters of the composite insertion pin

According to the structural form of the composite insertion pin and the actual insertion process of corn stalks, the main structural parameters included the sleeve contact-segment diameter d_1, steel pin working-segment diameter d_2, sleeve front transition angle α, first transition angle β, second transition angle γ, and actual stalk insertion depth S. The structural annotations are shown in Figure 5.

Among these parameters, d_1 and d_2 jointly affect the compression degree of the stalk pith, sidewall friction and holding stability. When the diameters are small, pith squeezing and friction are reduced, which is beneficial for decreasing the insertion force; however, the supporting effect of the insertion pin on the stalk is also weakened. When the diameters are large, the supporting effect is enhanced, but pith compression and contact friction increase accordingly, resulting in higher thrust of the push block.

The sleeve front transition angle α determines the smoothness of the transition when the sleeve enters the pith, directly affecting contact resistance and sudden changes in thrust. The first transition angle β and second transition angle γ mainly affect the structural transition and load transmission between different diameter sections of the sleeve. The insertion depth S represents the total length of the stalk sleeved onto the composite insertion pin along the axial direction. The parameters and their functions are listed in Table 1.

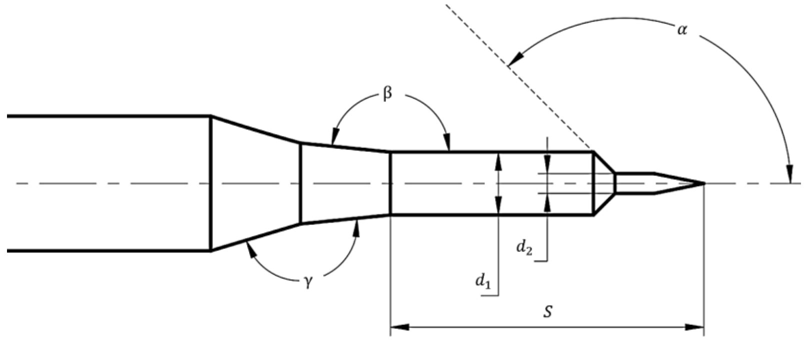

Fig. 5 - Structural parameters of the composite insertion pin

Table 1

Main structural parameters and functions of the composite insertion pin

Parameter	Symbol	Main function
Sleeve contact-segment diameter	d_1	Affects sleeve support stability and sidewall friction resistance
Steel pin working-segment diameter	d_2	Affects penetration resistance, compression resistance and insertion stability
Sleeve front transition angle	α	Affects the contact resistance and thrust fluctuation when the sleeve initially enters the stalk pith
First transition angle	β	Affects load transmission and structural transition at the variable-diameter section
Second transition angle	γ	Affects the structural transition and assembly stability of the rear connecting section
Actual stalk insertion depth	S	Represents the total depth of the stalk sleeved onto the composite insertion pin

Overall force model of the composite insertion pin

Under the action of an external axial load, the corn stalk moved along the axial direction of the insertion pin and was successively sleeved onto the steel pin working segment and the sleeve contact segment. Since the penetration of the steel pin into the stalk pith occurred simultaneously with local pith compression, these two effects were difficult to separate strictly. Therefore, they were collectively regarded as compression resistance. The total axial resistance acting on the composite insertion pin can be expressed by Eq. (1).

$$F_i = F_c + F_f \tag{1}$$

where $\boldsymbol{F_i}$ is the resultant axial force exerted by the stalk on the insertion pin, $\boldsymbol{F_c}$ is the compression resistance, and $\boldsymbol{F_f}$ is the sidewall friction force.

The sidewall friction force is related to the contact state between the insertion pin and the stalk pith and can be simplified by Eq. (2).

$$F_f = \mu p_n A_c \tag{2}$$

where $\boldsymbol{\mu}$ is the equivalent friction coefficient, $\boldsymbol{p_n}$ is the equivalent radial normal pressure, and $\boldsymbol{A_c}$ is the equivalent contact area between the insertion pin and the stalk pith. This equation indicates that increases in the pin diameter and contact length increase the sidewall friction force, thereby increasing the axial resistance during insertion.

During the actual insertion process, lateral force $\boldsymbol{F_y}$ may be generated by uneven stalk ends, non-uniform pith tissue distribution and eccentric loading. In this case, the vertical reaction force at the fixed end can be expressed by Eq. (3).

$$R_{Ay} = F_y \tag{3}$$

The bending moment at the fixed end can be calculated using Eq. (4).

$$M_A = F_i e + F_y l_y \tag{4}$$

where $\boldsymbol{e}$ is the eccentric distance of the resultant axial force relative to the centreline of the insertion pin, and $\boldsymbol{l_y}$ is the distance from the action point of the lateral force to the fixed end. Therefore, although the load mainly acts on the insertion region, its mechanical effect is transmitted to the entire composite insertion pin. The fixed end and the variable-diameter section are the key positions for structural verification.

Analysis of stalk release conditions

After the stalk is sleeved onto the insertion pin, smooth release should be ensured. Since the insertion pin has a smooth structure, the release process mainly needs to overcome the frictional resistance between the sidewall of the insertion pin and the stalk pith. Therefore, the release resistance can be approximated by Eq. (5).

$$F_d \approx F_f \tag{5}$$

To ensure smooth release of the stalk, the condition given in Eq. (6) should be satisfied.

$$F_r > F_d \tag{6}$$

where F_r is the release driving force, and F_d is the release resistance.

Optimization method for structural parameters of the composite insertion pin

To reduce the growth rate of insertion force while considering holding and release performance, the parameters of the composite insertion pin were determined using a procedure of "preliminary tests for range determination–Box-Behnken response surface optimization". Response surface methodology is suitable for analyzing the coupled effects of multiple factors, and the Box-Behnken design can establish a quadratic regression model and evaluate factor significance with fewer tests (*Box and Behnken, 1960; Myers et al., 2016; Montgomery, 2017*). In this study, the sleeve contact-segment diameter $\boldsymbol{d_1}$, steel pin diameter $\boldsymbol{d_2}$, and sleeve front transition angle $\boldsymbol{\alpha}$ were selected as factors, and the insertion force stiffness $\boldsymbol{K_F}$ was used as the response value. The factor levels were first determined through single-factor preliminary tests, and then modelling and optimization were performed using Design-Expert 13.

Insertion force stiffness $\boldsymbol{K_F}$ was selected as the continuous response because it directly characterizes the growth rate of insertion resistance. Holding stability and release performance were treated as functional constraints rather than continuous regression responses. Holding was considered successful when the stalk remained stably sleeved without obvious slipping after insertion, whereas release was considered successful when the stalk was completely detached without jamming, overall end splitting or visible bending of the insertion pin.

PARAMETER OPTIMISATION AND PERFORMANCE VERIFICATION OF THE COMPOSITE INSERTION PIN

Preliminary test design and determination of factor levels

Air-dried corn stalks with an average moisture content of 5.2% and diameters of 20–24 mm were used. Nine preliminary tests and 17 Box–Behnken tests were conducted independently, with a new stalk used in each test. The test system consisted of a screw-driven push block, composite insertion pin, support frame, RP-C30-ST resistive force sensor, voltage-conversion module and data-acquisition unit. The sensor had a nominal range of approximately 0.20–196 N and a sensing-area diameter of 25 mm.

RESULTS

Before testing, the sensor was calibrated, and its output was converted into force according to the calibration relationship. Force and displacement were recorded at 40 Hz during insertion to a depth of 30 mm at a speed of 0.1 m/s. The maximum insertion force $F_{p,\max}$ was extracted from each force–displacement curve, and K_F was calculated using Eq. (7).

Table 2

Preliminary test results of structural parameters of the composite insertion pin

Test No.	d_1/mm	d_2/mm	α /(°)	Test purpose	K_F/(N/mm)
1	6	2	155	Centre point	1.17
2	5	2	155	Low level of d_1	1.11
3	7	2	155	High level of d_1	1.66
4	6	1	155	Low level of d_2	1.28
5	6	3	155	High level of d_2	1.50
6	6	2	145	Low level of α	1.57
7	6	2	165	High level of α	1.21
8	6	2	155	Centre point replicate	1.13
9	6	2	155	Centre point replicate	1.18

The preliminary test results showed that the repeated center-point values were 1.17, 1.13 and 1.18 N/mm, indicating good repeatability. As d_1 increased, the insertion force stiffness increased markedly. K_F also showed an increasing trend with the increase in d_2, but the increment was smaller than that caused by d_1. In contrast, K_F decreased as **α** increased, indicating that a larger transition angle helped reduce the concentrated squeezing of the pith by the front end of the sleeve. These results show that the selected factor levels can be used for the subsequent response surface tests.

Evaluation index of insertion force stiffness

To quantitatively characterize the growth rate of insertion force with displacement, the insertion force stiffness K_F was introduced. Considering that the initial contact stage is strongly affected by uneven stalk ends and local compaction, whereas pith crushing, fiber failure or sudden changes in friction may occur near the peak force, the stable rising interval from $0.1F_{p,\max}$ to $0.8F_{p,\max}$ was selected for calculating K_F (*Mohsenin, 1986; Bourne, 2002; Rivera et al., 2022*). Accordingly, K_F was calculated using Eq. (7):

$$K_F = \frac{0.8F_{p,\max} - 0.1F_{p,\max}}{s_{0.8} - s_{0.1}} \tag{7}$$

where K_F (N/mm) is the insertion force stiffness; $F_{p,\max}$ (N) is the maximum insertion force; and $s_{0.1}$ and $s_{0.8}$ (mm) are the insertion displacements corresponding to $0.1F_{p,\max}$ and $0.8F_{p,\max}$, respectively.

Response surface test design

A three-factor and three-level response surface test was conducted using the Box-Behnken design in Design-Expert 13, with d_1, d_2 and α selected as the test factors. The insertion depth was fixed at 30 mm, and the push block speed was fixed at 0.1 m/s. The factor levels are listed in Table 3, and the test scheme and results are shown in Table 4.

Table 3

Factors and levels of the response surface test

Factor	Parameter	Low level -1	Centre level 0	High level +1
A	Sleeve contact-segment diameter d_1 / mm	5	6	7
B	Steel pin diameter d_2 / mm	1	2	3
C	Sleeve front transition angle α / °	145	155	165

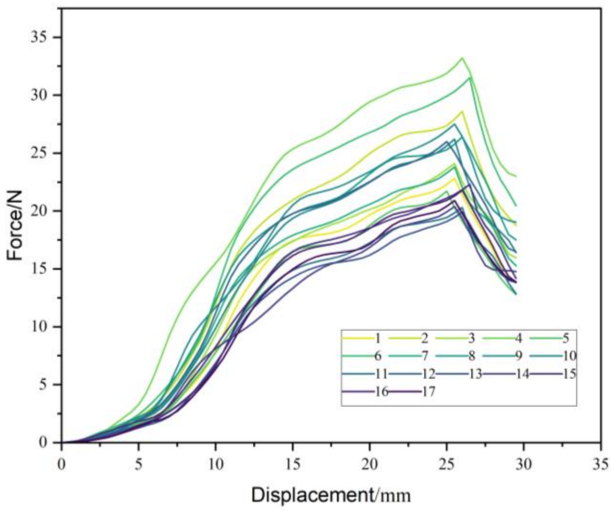

Fig. 6 - Force–displacement curves under different test groups

Table 4

Box-Behnken experimental design and results

Test No	A	B	C	K_F/(N/mm)
1	-1	-1	0	1.34
2	1	-1	0	1.65
3	-1	1	0	1.41
4	1	1	0	1.95
5	-1	0	-1	1.24
6	1	0	-1	1.86
7	-1	0	1	1.41
8	1	0	1	1.51
9	0	-1	-1	1.62
10	0	1	-1	1.55
11	0	-1	1	1.15
12	0	1	1	1.57
13	0	0	0	1.09
14	0	0	0	1.08
15	0	0	0	1.27
16	0	0	0	1.26
17	0	0	0	1.15

Among the 17 test groups, K_F ranged from 1.08 to 1.95 N/mm, indicating that the structural parameters had a significant effect on the growth rate of insertion force. The highest $\boldsymbol{K_F}$ value was 1.95 N/mm in test No. 4 ($\boldsymbol{d_1} = 7$ mm, $\boldsymbol{d_2} = 3$ mm and $\boldsymbol{\alpha} = 155°$). The repeated center-point values ranged from 1.08 to 1.27 N/mm, indicating a relatively small test error. Overall, $\mathbf{K_F}$ was lower near the center region and under some low-level parameter combinations, whereas it increased markedly under high-diameter combinations.

Regression model establishment and analysis of variance

Design-Expert 13 was used to conduct analysis of variance on the insertion force stiffness results, and the quadratic polynomial regression equation was obtained as follows: $\boldsymbol{K_F = 1.17 + 0.1963A + 0.09B - 0.0788C + 0.0575AB - 0.13AC + 0.1225BC + 0.225A^2 + 0.1925B^2 + 0.11C^2}$.

The regression equation shows that the coefficients of the linear terms $\boldsymbol{A}$ and $\boldsymbol{B}$ are positive, indicating that increases in $\boldsymbol{d_1}$ and $\boldsymbol{d_2}$ both increase the insertion force stiffness. The coefficient of $\boldsymbol{C}$ is negative, indicating that an appropriate increase in the transition angle is beneficial for reducing the insertion force stiffness. The quadratic terms $\boldsymbol{A^2}$, $\boldsymbol{B^2}$and $\boldsymbol{C^2}$are all positive, suggesting obvious nonlinear effects of the factors on $\boldsymbol{K_F}$. Therefore, a lower optimization region exists in the response surface.

Table 5

Analysis of variance for the regression model

Source	Sum of squares	df	Mean square	F-value	p-value	Significance
Model	1.03	9	0.1142	18.06	0.0005	**
A	0.3081	1	0.3081	48.71	0.0002	**
B	0.0648	1	0.0648	10.25	0.0150	*
C	0.0496	1	0.0496	7.84	0.0265	*
AB	0.0132	1	0.0132	2.09	0.1914	
AC	0.0676	1	0.0676	10.69	0.0137	*
BC	0.0600	1	0.0600	9.49	0.0178	*
A^2	0.2132	1	0.2132	33.70	0.0007	**
B^2	0.1560	1	0.1560	24.67	0.0016	**
C^2	0.0509	1	0.0509	8.05	0.0251	*
Residual	0.0443	7	0.0063			
Lack of fit	0.0113	3	0.0038	0.4556	0.7278	
Pure error	0.0330	4	0.0083			
Total	1.07	16				
R^2	0.9587					
R^2_{Adj}	0.9056					

Note: * indicates significant difference at $P < 0.05$; ** indicates highly significant difference at $P < 0.01$.

The analysis of variance showed that the model was highly significant, with $P = 0.0005 < 0.01$. The lack-of-fit term was not significant ($P = 0.7278 > 0.05$), indicating that the model fitted the test data well. The values of R^2 and R^2_{adj} were 0.9587 and 0.9056, respectively, further confirming the good fitting performance of the model. Factor A had a highly significant effect on K_F, while factors B and C also had significant effects. This indicates that the sleeve contact-segment diameter had the greatest influence on K_F, followed by the steel pin diameter and the sleeve front transition angle. Among the interaction terms, AC and BC were significant.

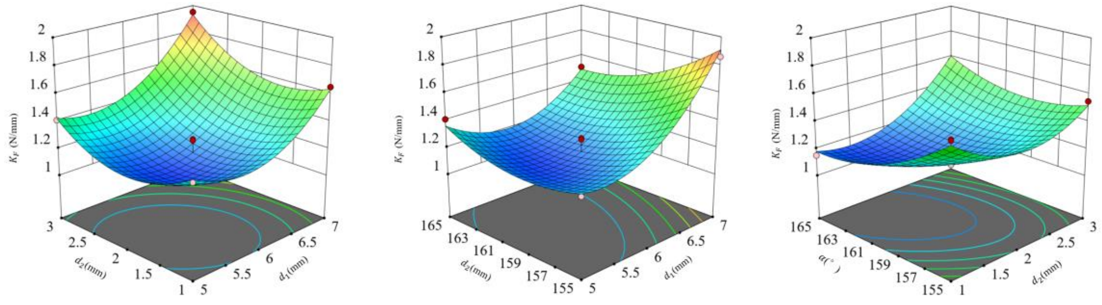

Fig. 7 - Effects of response surface interactions on insertion force stiffness

a) A-B; b) A-C; c) B-C

Parameter optimization and engineering recommended values

The regression model showed that the theoretical optimal parameter region was approximately $d_1 = 5.70$ mm, $d_2 = 1.70$ mm and $\alpha = 158.5°$, with a predicted insertion force stiffness of about 1.11 N/mm. Considering practical machining requirements, $d_1 = 5.5$ mm, $d_2 = 2.0$ mm and $\alpha = 160°$ were finally selected as the engineering recommended parameter combination. Under this combination, the predicted insertion force stiffness was approximately 1.15 N/mm. Its prediction accuracy was subsequently evaluated through internodal insertion tests, whereas nodal insertion and release tests were conducted to assess high-resistance adaptability and functional reliability.

According to the axial force model in Section 3, the insertion force mainly consisted of pith compression resistance and sidewall friction resistance. The steel pin diameter, sleeve contact-segment diameter and sleeve front transition angle affected pith compression, sidewall friction and guided compression, respectively. The response surface results were consistent with the theoretical analysis, indicating that the established model can provide a basis for structural parameter optimization of the composite insertion pin.

It should be noted that the response surface optimization was mainly used to obtain a low-resistance parameter combination under regular axial insertion conditions. Since the nodal region has denser tissue and a transverse diaphragm, stronger local resistance fluctuations occur during insertion. Therefore, nodal insertion was used as a high-resistance adaptability verification of the recommended parameter combination, rather than to evaluate the prediction accuracy of the response surface regression model.

PERFORMANCE VERIFICATION OF THE COMPOSITE INSERTION PIN

Finite element analysis of bending resistance of the composite insertion pin

Static structural analysis was conducted in ANSYS Workbench to evaluate the bending stability of the optimized composite insertion pin. Bonded contacts were defined at the interfaces among the steel pin, steel shaft, PETG sleeve and support. The PETG support base was fixed to represent its frame connection, and a lateral load of 20 N was applied at the pin tip.

Table 6

Mesh convergence results

Element size /mm	Nodes	Elements	Deformation /mm	Average stress /MPa
0.30	1,256,239	730,860	1.9039	1.6589
0.25	1,818,875	1,060,416	2.0224	1.7260
0.20	2,838,580	1,658,786	2.0020	1.7159

The differences between the 0.25 and 0.20 mm meshes were 1.02% for maximum deformation and 0.59% for area-averaged equivalent stress; therefore, the 0.20 mm mesh was adopted. As shown in Figure 8, the maximum deformation was 2.00 mm, while the maximum equivalent stresses of the whole model and PETG sleeve were 196.2 and 36.09 MPa, respectively. Based on yield strengths of 355 MPa for steel and 45 MPa for PETG, the corresponding safety factors were 1.81 and 1.25, indicating that no yielding was predicted under the applied load.

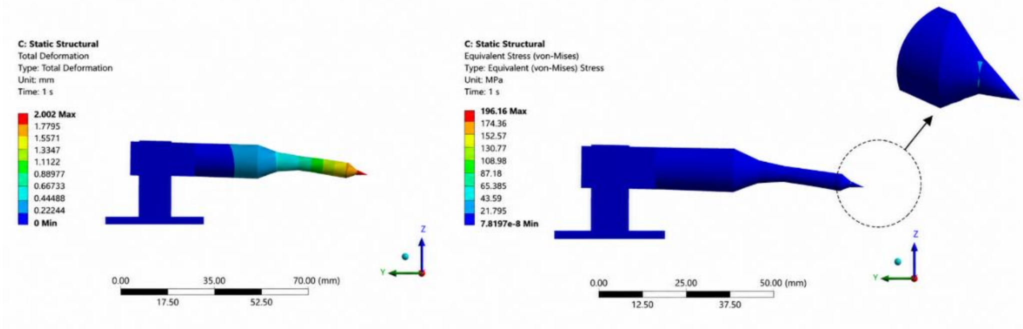

a) b)

Fig. 8 - Finite element analysis results of the bending resistance of the composite insertion pin

a) total deformation contour; b) equivalent stress contour

The PETG transition region could be strengthened by increasing the fillet radius and wall thickness, while its mechanical properties could also be improved by optimizing the printing parameters (*Szykiedans et al., 2017; Özen et al., 2021; Tunçel et al., 2024*).

Internodal and nodal insertion verification tests

To directly validate the recommended parameter combination under regular internodal insertion conditions and evaluate its adaptability to the nodal region, five independent internodal and five independent nodal axial insertion tests were conducted. The composite insertion pin with $\boldsymbol{d_1} = 5.5$ mm, $\boldsymbol{d_2} = 2.0$ mm and $\boldsymbol{\alpha} = 160°$ was used. The insertion depth was 30 mm, and the force–displacement curve, maximum insertion force, insertion force stiffness and end failure condition were recorded.

Table 7

Verification test results of axial insertion in the internodal and nodal regions

Test No	Insertion depth /mm	Internodal $F_{p,\max}$ /N	Internodal K_F/(N/mm)	Nodal $F_{p,\max}$ /N	Nodal K_F/(N/mm)
1	30	39.2	1.12	68.7	2.12
2	30	40.1	1.16	70.1	2.18
3	30	38.7	1.15	71.4	2.25
4	30	41.0	1.19	69.3	2.16
5	30	39.6	1.14	72.0	2.31

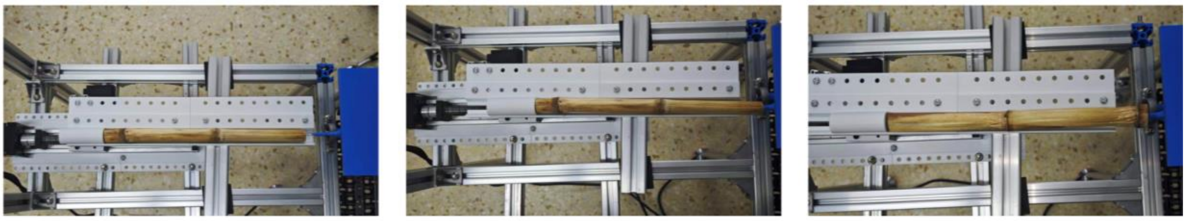

a） b） c）

Fig. 9 - Verification tests of axial insertion in the internodal and nodal regions
a) insertion test device and initial state; b) axial insertion process in the internodal region; c) state after insertion in the nodal region

Table 7 and Figure 9 show that the optimized composite insertion pin completed 30 mm axial insertion in all internodal and nodal tests. Under regular internodal insertion, the measured $\boldsymbol{K_F}$ was 1.15 ± 0.03 N/mm, with a relative error of 0.17% from the predicted value of 1.15 N/mm, confirming the prediction accuracy of the response surface model. In the nodal region, $\boldsymbol{F_{p,\max}}$ and $\boldsymbol{K_F}$ increased to 70.3 ± 1.4N and 2.20 ± 0.08 N/mm, respectively, owing to the dense tissue and transverse diaphragm. Nevertheless, no obvious bending of the insertion pin, overall splitting of the stalk or interruption of the insertion process was observed.

Stalk release function verification

To evaluate the holding stability and release performance of the optimized composite insertion pin, repeated release tests were conducted using stalks pre-sleeved in the internodal and nodal regions. The composite insertion pin with $\boldsymbol{d_1} = 5.5$ mm, $\boldsymbol{d_2} = 2.0$ mm and $\boldsymbol{\alpha} = 160°$ was used. After being pre-sleeved to a depth of 30 mm, each stalk was axially released by the release mechanism. Holding was considered successful when the stalk remained stably sleeved without visible slipping, whereas release was considered successful when the stalk was completely detached without jamming, overall end splitting or visible bending of the insertion pin. The holding state, release state and possible failure phenomena were recorded.

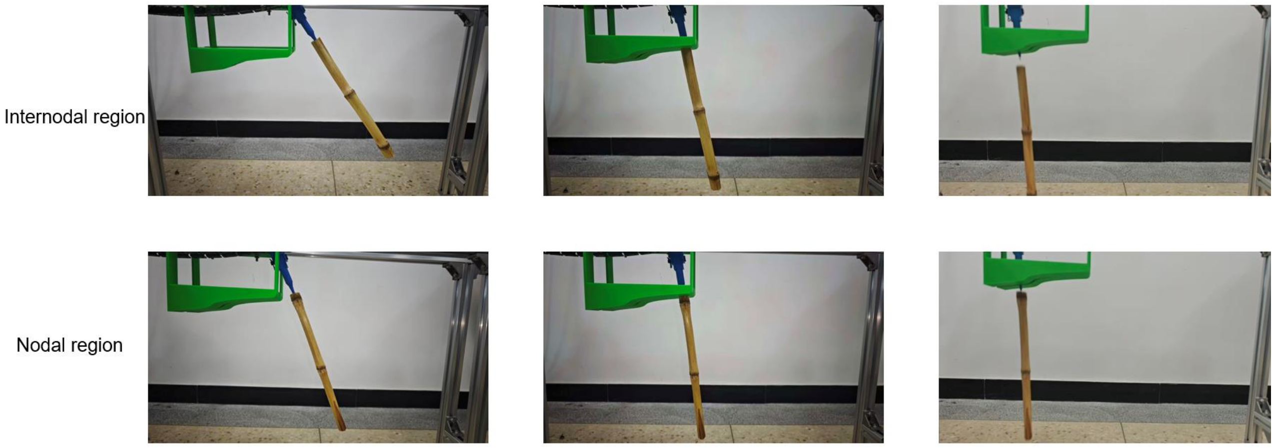

Fig. 10 - Stalk release verification test results

As shown in Figure 10, stable holding and complete release were achieved in both the internodal and nodal tests. No visible slipping, jamming, overall end splitting, bending of the insertion pin or structural damage was observed. Although the local contact resistance was higher in the nodal region, complete release was still achieved, indicating that the optimized composite insertion pin satisfied the requirements for stable holding and smooth release after axial insertion.

CONCLUSIONS

This study designed and optimized a smooth composite insertion pin consisting of a front steel pin and a rear sleeve to solve the problems of high resistance, obvious force fluctuation near nodes and poor release during axial insertion of corn stalks. The main conclusions are as follows:

(1) A smooth composite insertion pin consisting of a front steel pin and a rear sleeve was designed according to the heterogeneous structural characteristics of corn stalks. The structure enabled axial insertion, stable sleeving and subsequent release while reducing end crushing and overall stalk splitting.

(2) The axial insertion force was mainly composed of pith compression resistance and sidewall friction. The sleeve contact-segment diameter $\boldsymbol{d_1}$, steel pin diameter $\boldsymbol{d_2}$ and sleeve front transition angle $\boldsymbol{\alpha}$ affected sidewall friction, pith compression and guided compression, respectively, providing a theoretical basis for parameter optimization.

(3) The Box–Behnken regression model was highly significant, whereas the lack-of-fit term was not significant, with $\boldsymbol{R^2} = 0.9587$ and $\boldsymbol{R^2_{\text{adj}}} = 0.9056$. The sleeve contact-segment diameter had the greatest effect on $\boldsymbol{K_F}$, while the steel pin diameter and transition angle also had significant effects.

(4) Considering response surface optimization, machining feasibility and structural stability, the engineering parameters were determined as $\boldsymbol{d_1} = 5.5$ mm, $\boldsymbol{d_2} = 2.0$ mm and $\boldsymbol{\alpha} = 160°$, with a predicted $\boldsymbol{K_F}$ of approximately 1.15 N/mm. Five internodal validation tests gave a measured $\boldsymbol{K_F}$ of 1.15 ± 0.03 N/mm, with a relative prediction error of 0.17%, indicating good agreement between the measured and predicted results.

(5) Finite element analysis showed that the optimized structure maintained acceptable bending stability under the applied lateral load. In nodal insertion tests, the maximum insertion force increased to approximately 70 N, but no obvious bending, overall stalk splitting or insertion interruption occurred. Holding and release tests further confirmed stable sleeving and complete release in both internodal and nodal regions. However, the present study was limited to laboratory tests over a narrow moisture-content and diameter range, and dynamic impact and fatigue during continuous field operation were not considered. Future work will focus on multi-condition field tests and continuous-operation verification.

ACKNOWLEDGEMENT

The authors were funded for this project by the National Natural Science Foundation of China (NSFC), Grant/Award Number: 52265039.

REFERENCES

[1] An R., Ge Y., Zheng Y.J., Cheng J.J., Zeng X.Y., Jin M.Y., (2025), Transverse intermittent straw-pressing mechanism of the paving machine for reed straw checkerboard. *Transactions of the Chinese Society of Agricultural Engineering*, Vol.41(7), pp.36-46.

[2] Bourne M.C., (2002), *Food Texture and Viscosity: Concept and Measurement*, 2nd ed., Academic Press, San Diego/USA.

[3] Box G.E.P., Behnken D.W., (1960), Some new three level designs for the study of quantitative variables. *Technometrics*, Vol.2(4), pp.455-475.

[4] Chen Y.F., Wang F., Pan X.B., Zhang F.M., Ren G.Y., Li Q., (2024), 150-year shift of potential geographical distribution of desertification in China: Past, present and future (中国荒漠化潜在发生区域 150 年变迁: 过去、现在和未来), *Chinese Science Bulletin*, Vol.69(31), pp.4637-4650.

[5] Chen Z., Qu G., (2017), Shearing characteristics of corn stalk pith for separation. *BioResources*, Vol.12(2), pp.2296-2309.

[6] Coetzee C.J., (2017), Review: Calibration of the discrete element method. *Powder Technology*, Vol.310, pp.104-142.

[7] Cook D.D., Meehan K., Asatiani L., Robertson D.J., (2020), The effect of probe geometry on rind puncture resistance testing of maize stalks. *Plant Methods*, Vol.16, pp.65.

[8] Cundall P.A., Strack O.D.L., (1979), A discrete numerical model for granular assemblies. *Géotechnique*, Vol.29(1), pp.47-65.
[9] Fang W., Li S.X., Jiang Y.J., Dong W.J., (2023), Research on the effect of sand barriers on highways in desert areas on sand control. *Sustainability*, Vol.15, pp.13906.
[10] Liu Y.N., Li Y.X., Han X.Q., Yang Q.W., Yang D.M., Tao H.J., (2025), Analysis of the effectiveness of four types of banded sand barriers in the Ulan Buh Desert (乌兰布和沙漠 4 种带状沙障建设成效分析), *Journal of Inner Mongolia Forestry Science & Technology*, Vol.51(1), pp.1-6.
[11] Mohsenin N.N., (1986), *Physical Properties of Plant and Animal Materials*, 2nd ed., Gordon and Breach Science Publishers, New York/USA.
[12] Montgomery D.C., (2017), *Design and Analysis of Experiments*, 9th ed., John Wiley & Sons, Hoboken/USA.
[13] Myers R.H., Montgomery D.C., Anderson-Cook C.M., (2016), *Response Surface Methodology: Process and Product Optimization Using Designed Experiments*, 4th ed., John Wiley & Sons, Hoboken/USA.
[14] Özen A., Auhl D., Völlmecke C., Kiendl J., Abali B.E., (2021), Optimization of Manufacturing Parameters and Tensile Specimen Geometry for Fused Deposition Modeling (FDM) 3D-Printed PETG. *Materials*, Vol.14(10), pp.2556.
[15] Qi Y., Kong D., Zhang P., Zhang Y., Zheng X., Su Y., Ma X., Sun B., (2025), Design and Optimization of a Compact Machine for Laying and Pressing Straw Checkerboard Sand Barriers in Desert Areas. *Agriculture*, Vol.15(17), pp.1818.
[16] Qu J.J., Ling Y.Q., Liu B.J., Chen G.T., Wang T., Dong Z.B., (2019), Research status and development trend of wind-blown sand control engineering in China (我国风沙防治工程研究现状及发展趋势). Advances in Earth Science, Vol.34(3), pp.225-231.
[17] Rivera S., Giongo L., Cappai F., Kerckhoffs H., Sofkova-Bobcheva S., Hutchins D., East A., (2022), Blueberry firmness: A review of the textural and mechanical properties used in quality evaluations. *Postharvest Biology and Technology*, Vol.192, pp.112016.
[18] Robertson D.J., Julias M., Lee S.Y., Cook D.D., (2016), Maize stalk lodging: flexural stiffness predicts strength. *Crop Science*, Vol.56(4), pp.1711-1718.
[19] Stubbs C.J., McMahan C.S., Tabaracci K., Kunduru B., Sekhon R.S., Robertson D.J., (2022), Cross-sectional geometry predicts failure location in maize stalks. *Plant Methods*, Vol.18, Article 56.
[20] Sun J., Shen W., Li Y.Z., Ma J.J., Huang J.Z., Wang J., Chen P., Li H.B., Zhang B.Y., Li Y., (2024), Experimental study on a combined sand barrier: Integration of porous mesh plate and novel porous sand-fixing bricks. *Journal of Wind Engineering & Industrial Aerodynamics*, Vol.251, pp.105809.
[21] Szykiedans K., Credo W., Osiński D., (2017), Selected mechanical properties of PETG 3-D prints. *Procedia Engineering*, Vol.177, pp.455-461.
[22] Tsuji Y., Tanaka T., Ishida T., (1992), Lagrangian numerical simulation of plug flow of cohesionless particles in a horizontal pipe. *Powder Technology*, Vol.71(3), pp.239-250.
[23] Tunçel O., Kahya Ç., Tüfekci K., (2024), Optimization of Flexural Performance of PETG Samples Produced by Fused Filament Fabrication with Response Surface Method. *Polymers*, Vol.16(14), pp.2020.
[24] Wang T., Qu J.J., Ling Y.Q., Liu B.L., Xiao J.H., (2018), Shelter effect efficacy of sand fences: A comparison of systems in a wind tunnel. *Aeolian Research*, Vol.30, pp.32-40.
[25] Wang Y., Jiang A.F., Jiang J.Z., (2024), Numerical Simulation and Parameter Optimization of a New Slant Insertion-Opening Combination Sand Fence. *Sustainability*, Vol.16, pp.8651.
[26] Xu G.W., He N., Zhang J., Dong H.C., (2021), Investigations into the design of sand control fence for Gobi buildings. *Aeolian Research*, Vol.49, pp.100662.
[27] Xu X.Y., Zhao P., Tang J.N., Ji Y.F., Ma X.B., (2020), Research and development status and prospect of sand control machinery in China (我国治沙机械研发现状与展望). Forestry and Grassland Machinery, Vol.1(2), pp.21-25.
[28] Zhang K., Zhang P.W., Zhang J.C., Zhang X.X., (2021), Protective effect of multi-row HDPE board sand fences: A wind tunnel study. *International Soil and Water Conservation Research*, Vol.9(1), pp.103-115.
[29] Zhang L., Sun B.G., Zhang K.P., Zhang P., Qi Y., Kong D.R., (2022), Research status and prospect of sand control machines in China (我国治沙机器的研究现状与展望). Forestry Machinery & Woodworking Equipment, Vol.50(12), pp.4-8.

[30] Zhang L., Yang Z., Zhang Q., Guo H., (2016), Tensile properties of maize stalk rind. *BioResources*, Vol.11(3), pp.6151-6161.
[31] Zhang S., Ding G.D., Yu M.H., Gao G.L., Zhao Y.Y., Wu G.H., Wang L., (2018), Effect of straw checkerboards on wind proofing, sand fixation, and ecological restoration in shifting sandy land. *International Journal of Environmental Research and Public Health*, Vol.15(10), pp.2184.
[32] Zhang T., Zhao M.Q., Liu F., Tian H.Q., Wulan T., Yue Y., Li D.P., (2020), A discrete element method model of corn stalk and its mechanical characteristic parameters. *BioResources*, Vol.15(4), pp.9337-9350.
[33] Zhao C.L., Li Q., Zhou N., Zhang J.Q., Kang L.Q., Shen Y.P., Jia W.R., (2016), Field observations of wind profiles and sand fluxes above the windward slope of a sand dune before and after the establishment of semi-buried straw checkerboard barriers. *Aeolian Research*, Vol.20, pp.59-70.
[34] Zhu H.P., Zhou Z.Y., Yang R.Y., Yu A.B., (2007), Discrete particle simulation of particulate systems: Theoretical developments. *Chemical Engineering Science*, Vol.62(13), pp.3378-3396.